Journal of Alloys and Compounds 781 (2019) 118–130

Contents lists available at ScienceDirect

Journal of Alloys and Compounds

journal homepage: http://www.elsevier.com/locate/jalcom

Effects of Ce and Y addition on microstructure evolution and precipitation of Cu-Mg alloy hot deformation

Bingjie Wang [a, b], Yi Zhang [a, b, *], Baohong Tian [a, b, **], Vladislav Yakubov [c], Junchao An [b, d], Alex A. Volinsky [c], Yong Liu [a, b], Kexing Song [a, b], Lihua Li [a, b], Ming Fu [e]

[a] School of Materials Science and Engineering, Henan University of Science and Technology, Luoyang 471023, PR China
[b] Collaborative Innovation Center of Nonferrous Metals, Henan Province, Luoyang 471023, PR China
[c] Department of Mechanical Engineering, University of South Florida, Tampa 33620, USA
[d] School of Materials Science and Engineering, Luoyang Institute of Science and Technology, Luoyang 471023, PR China
[e] Luoyang Electro-Optics Technology Development Centre, Luoyang 471023, PR China

ARTICLE INFO

Article history:
Received 10 September 2018
Received in revised form
16 November 2018
Accepted 3 December 2018
Available online 4 December 2018

Keywords:
Hot compression
Flow stress
Critical strain
Microstructure evolution
Twinning mechanism

ABSTRACT

The effects of Ce and Y addition on microstructure evolution and precipitation of Cu-Mg alloy hot deformation were investigated by hot compression test in the 500–850 °C temperature range and the 0.001–10 s^{-1} strain rate range. The influence of rare earth elements on true stress-true strain curves and microstructure evolution of Cu-Mg alloy were obtained, the deformation mechanism under various conditions was defined, and the critical strain of Cu-Mg, Cu-Mg-Ce, and Cu-Mg-Y alloys and the resulting precipitates were determined. Dynamic recrystallization dominated the deformation process at high temperature and low strain rate. Ce and Y significantly delayed dynamic recrystallization and improved flow stress and activation energy of Cu-Mg alloy. The critical strains for Cu-Mg, Cu-Mg-Ce, and Cu-Mg-Y alloys deformed at 700 °C and 0.1 s^{-1} were calculated to be 0.075, 0.1, and 0.14, respectively. Precipitates appeared in the Cu-Mg-Ce and Cu-Mg-Y alloys deformed at 850 °C and 0.001 s^{-1}, which were determined to be Cu_2Mg. In addition, CuP_2 phase was found in both Cu-Mg-Ce and Cu-Mg-Y alloys deformed at 800 °C and 0.01 s^{-1}. Precipitates caused dislocation and grain boundary pinning. Furthermore, a large number of twins appeared in the Cu-Mg-Ce and Cu-Mg-Y alloys, which increased the number of grain boundaries and furthered grain refinement.

1. Introduction

Copper alloys are widely used as materials for railway contact wires and lead frames due to the high strength, excellent conductivity, and favorable corrosion resistance properties. Currently, the most common way to improve copper-based material performance is by alloying them with elements such as Fe, P, Mg, Cr, and Zn. For example, railway contact wires use Cu-Mg and Cu-Sn alloys [1,2], while lead frames use Cu-Cr-Zr and Cu-Fe-P alloys [3,4].

Hot working process for the Cu alloys have been further investigated. Spigarelli et al. [5] analyzed the hot workability of Cu-Zn alloys and obtained a self-consistent constitutive model suitable for Cu-Zn alloy. Meanwhile, it proved the existence of hard and soft phases and also confirmed the addition of Zn causes decrease in stacking fault energy. Spigarelli and Mehtedi [6] found that the activation energy for hot working slowly decreased with increasing strain and lead to thermally activated flow softening. Similar phenomenon has been observed by Spigarelli. et al. [7] in 2205 duplex stainless steel during high temperature deformation. A mathematical model was established to illustrate the transition from this initial configuration to the final condition and successfully describe the characteristics of flow curves.

Jiang et al. [8] proved that the element of Sn has the effect of decreasing flow stress. Dong et al. [9] confirmed that the addition of Fe and P elements increased the tensile strength of Cu-0.7Fe-0.15P alloy. Due to the positive effect of rare earth elements on copper alloy properties, the addition of rare earth elements has become a hot research topic in recent years [10]. Stanford et al. [11,12] confirmed that addition of Ce leads to decreased yield point and

* Corresponding author. School of Materials Science and Engineering, Henan University of Science and Technology, Luoyang 471023, PR China.
** Corresponding author. School of Materials Science and Engineering, Henan University of Science and Technology, Luoyang 471023, PR China.
E-mail addresses: zhshgu436@163.com (Y. Zhang), tianbh@haust.edu.cn (B. Tian).

https://doi.org/10.1016/j.jallcom.2018.12.022
0925-8388/

increased ductility. Li et al. [13] demonstrated that the recrystallization temperature of pure copper rose with increasing Ce content, and the addition of trace Ce to cast pure copper caused fine-grain strengthening. Zhang et al. [14] investigated the addition of Y element to Cu-Cr-Zr and proved that Y caused copper matrix grain refinement, which increased material's strength and hardness. Chen et al. [15] studied the addition of Y to Cu-Zr-Al ternary alloy and found that Y increased the compressive strength and elastic strain limits. These results indicate that the addition of Ce and Y can improve the mechanical properties of alloys.

On the basis of above researches, fine-grain strengthening, enhancement of alloy properties and different precipitates were observed with the addition of Ce or Y. However, there is no specific discussion on the effect of dynamic recrystallization and activation energy of hot deformation. In this experiment, the effects of Ce and Y added to Cu-Mg alloy on hot processing properties were compared. Hot compression tests at 500–850 °C deformation temperature and 0.001–10 s^{-1} strain rate were carried out, and mechanisms for flow stress and activation energy change caused by Ce and Y addition were explained. The critical strain was calculated to determine the occurrence of dynamic recrystallization. The hot deformation microstructure evolution for Cu-Mg-Ce and Cu-Mg-Y alloys and the secondary phase was investigated. Deformation activation energy was obtained. The effects of twinning mechanism for Cu-Mg, Cu-Mg-Ce, and Cu-Mg-Y alloys properties were analyzed, respectively.

2. Experiment

Pure Cu, Mg, Sn, Y and master alloys Cu-10%Fe, Cu-12%P, Cu-19% Ce were used as raw materials, which were melted at 1200 ± 10 °C using a vacuum melting furnace with crucible dimensions of 89 mm ID, 20 mm OD, and 190 mm length. An argon atmosphere was used during melting to prevent material oxidation, and ingots created by the vacuum melting furnace were left to solidify before heating for 2 h at 900 °C for extrusion into a Φ35 mm cylinder using an XJ-500 metal profile extrusion machine. The extruded cylinder was then air cooled and machined into Φ8 × 12 mm cylinders suitable for hot compression testing, which was conducted utilizing the Gleeble-1500D thermo-mechanical simulator. Based on the practical production, cracks tend to occur below 500 °C with high strain rates. Hot deformation temperature of Cu-based alloy usually selected as 500–850 °C. According to the Cu-Mg phase diagram in Fig. 1, the phases at room temperature are α and Cu_2Mg. Thus, the deformation temperature was selected as 500 °C–850 °C and the strain rate was 0.001 s^{-1} to 10 s^{-1}. The samples were heated to a target deformation temperature at a heating rate of 10 °C/s and held at the target temperature for 3 min before undergoing 55% compression. Deformed samples were quenched in water within 2 s to keep the high temperature microstructure. In order to minimize the frictions, improve the uniformity and stability during the hot deformation, the tantalum foils with thickness of 0.1 mm were used between anvils and the specimen surfaces. After hot deformation, there is a 3–5 s interval between unloading and quenching. Alloy composition analysis is given in Table 1.

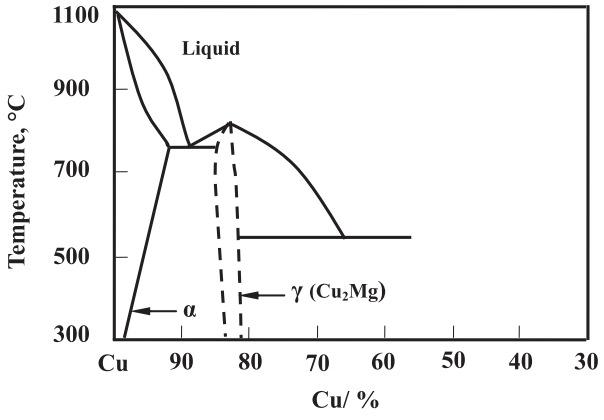

Fig. 1. Cu-Mg phase diagram.

Samples were cut parallel to the direction of deformation. Select the central part of each samples, polished, and then etched with solution (5 g $FeCl_3$, 10 mL HCl, 100 mL distilled water) for microstructure observation by using OLYMPUS PMG3 optical microscope. 3 mm diameter and 50 μm thick samples were prepared for TEM through ion thinning by using Gatan 691 ion beam thinner with incident angle of 9° and 5 keV ion beam energy. After a small hole was created by initial ion thinning, operating parameters of ion beam thinner were changed to 5° incident angle and 4 keV ion beam energy. Transmission electron microscope (JEM-2100) was used to analyze the precipitated phases and microstructure. The hardness of samples was tested using the HVS-1000 hardness tester, and each sample was measured 6 times to obtain an average value. Measurement error was calculated statistically to be within 10%.

3. Results

Fig. 2(a), (b) and (c) show the as-cast microstructure of the Cu-Mg, Cu-Mg-Ce, and Cu-Mg-Y alloys, respectively. Due to the fast cooling rate, the internal composition of the solid solution is not uniform. As a result, large number of dendrites appeared in the matrix. The corresponding microstructure of the three alloys after extrusion are shown in Fig. 2(d), (e) and (f). It can be concluded that high temperature extrusion after homogenization annealing can eliminate dendrite segregation and make the structure more homogeneous.

3.1. Flow stress

The most obvious characteristic of hot deformation is the change of flow stress, and material characteristics are altered by work hardening, dynamic recovery, and dynamic recrystallization. In order to understand the relationship between work hardening, dynamic recovery, and dynamic recrystallization, the true stress true strain curve was obtained by using the software Origin 2017. In the early stage of hot deformation, flow stress increases rapidly, which represents work hardening. Work hardening can lead to an increase in dislocation density, which in turn promotes dynamic recovery and dynamic recrystallization [16–18]. Then, the flow stress is gradually reduced. Fig. 3(a) illustrates the flows stress under various deformation strain rates at 800 °C. It can be seen that the flow stress increased rapidly in the early deformation stage and further increased with increasing strain rate [19]. The true stress of the three alloys increased to an obvious maximum value and then fell before reaching a stable value, which is a typical characteristic of dynamic recrystallization. Similar phenomenon can be seen in Fig. 3(b) as the alloys deformed at 850 °C. High temperature is more conducive to dynamic recrystallization. More obvious dynamic recrystallization grains were observed at the higher temperature.

Fig. 3(c) and (d) shows the flow stress of the three alloys deformed at 0.1 s^{-1} and 1 s^{-1} at various deformation temperatures. The flow stress decreases with decreasing deformation temperature. The peak stress of Cu-Mg, Cu-Mg-Ce, and Cu-Mg-Y alloys deformed at 600 °C and 0.1 s^{-1} strain rate is 157 MPa, 186 MPa, and 196 MPa, respectively. The corresponding peak stress value of the

Table 1
Alloy compositions analysis.

Nominal composition (wt. %)	Analyzed composition (wt. %)					
	Mg (%)	Sn (%)	Fe (%)	P (%)	Y (%)	Ce (%)
Cu-0.4%Mg-0.2%Sn- 0.2%Fe-0.15%P	0.383	0.198	0.209	0.143	–	–
Cu-0.4%Mg-0.2%Sn-0.2%Fe-0.15%P-0.15%Ce	0.392	0.221	0.192	0.149	–	0.141
Cu-0.4%Mg-0.2%Sn-0.2%Fe-0.15%P-0.15%Y	0.401	0.192	0.186	0.151	0.146	–

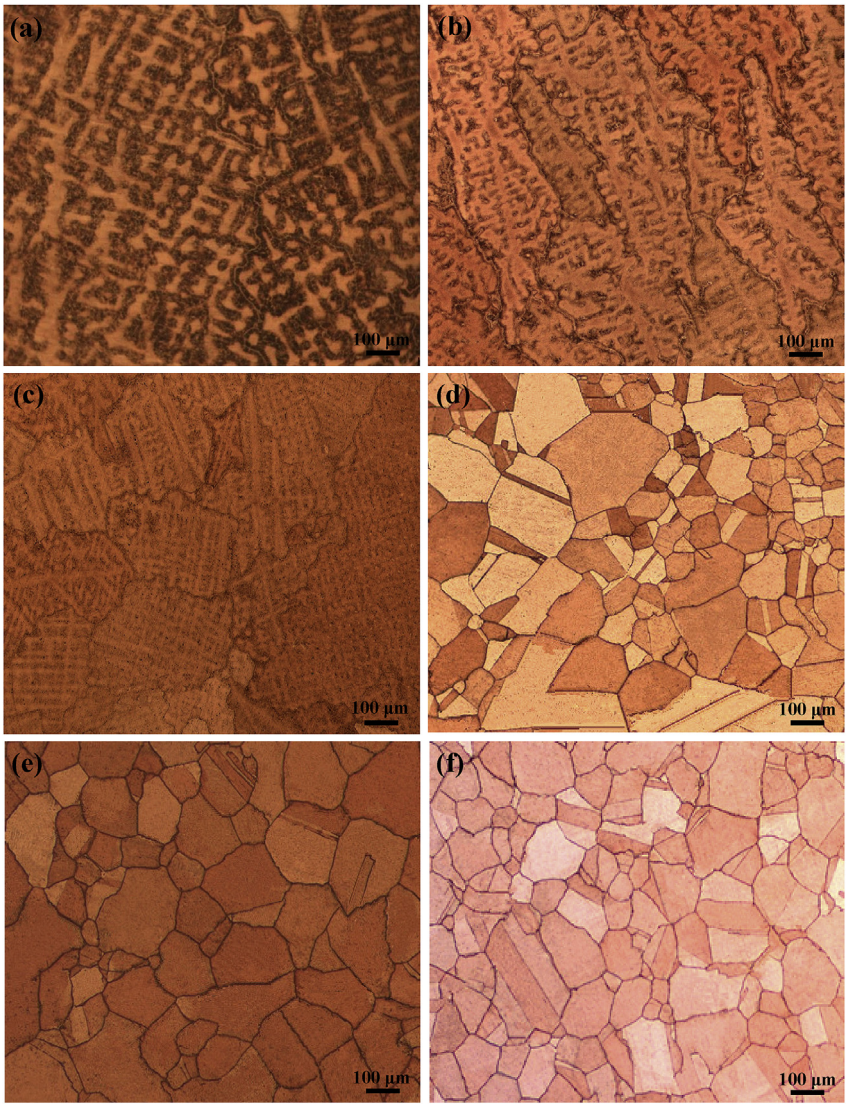

Fig. 2. Microstructure of (a) as-cast Cu-Mg alloy; (b) as-cast Cu-Mg-Ce alloy; (c) as-cast Cu-Mg-Y alloy; extruded at 900 °C (d) Cu-Mg alloy; (e) Cu-Mg-Ce alloy; (f) Cu-Mg-Y alloy.

three alloys at 600 °C and 1 s^{-1} is 202 MPa, 223 MPa, and 235 MPa, respectively. These values are higher than the values of lower strain at 600 °C. The reason for true stress-true strain curves exhibit typical dynamic recrystallization behavior at higher temperature and lower strain rate is that higher temperature or lower strain rate provide enough time energy accumulation and high boundary migration. Dynamic recrystallization controls deformation process. Therefore, dynamic softening is higher than work hardening. Meanwhile the flow stress for Cu-Mg-Ce and Cu-Mg-Y increased 10% and 16% compared with the Cu-Mg alloy tested at the same conditions. The above phenomenon can be analyzed based on the microstructure observations.

Fig. 4(a) illustrates the microstructure of the Cu-Mg alloy deformed at 500 °C and 1 s^{-1} strain rate. The shear bands were observed from Fig. 4(a) marked by the black circle and magnified in Fig. 4(b). The grains are elongated parallel to the direction of deformation, and the grain boundaries become blurred. It means the emergence of strain gathering area causes stress concentration and leads to work hardening. Therefore, the flow stress rises rapidly. As shown in Fig. 4(c), the matrix of the Cu-Mg alloy mainly consists of necklace structure deformed at 800 °C under the strain rate of 1 s^{-1}, which indicates that the rate of dynamic recrystallization increase rapidly for the alloy at this condition. The magnified view of the selected area is illustrated in Fig. 4(d). Plentiful dynamic

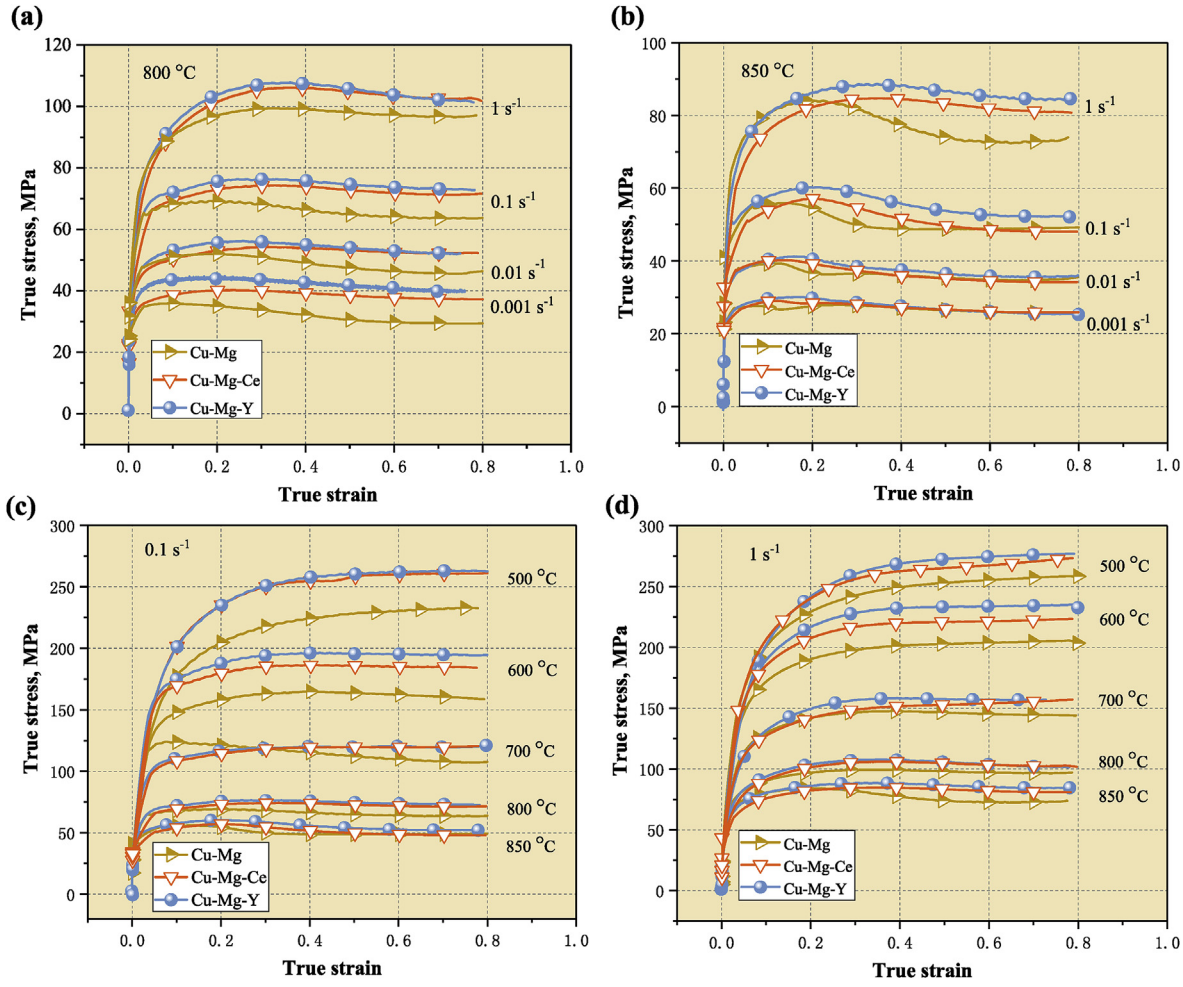

Fig. 3. True stress-true strain curves of Cu-Mg, Cu-Mg-Ce and Cu-Mg-Y alloys deformed at (a) 800 °C; (b) 850 °C; (c) 0.1 s^{-1}; (d) 1 s^{-1}.

recrystallized grains nucleared at grain boundaries and continue to consume distortion energy at grain boundaries. Thus, the work hardening process is gradually eliminated and the peak stress decreases.

In addition, many researchers have demonstrated that the rare earth element accelerates the precipitation of secondary phase and causes precipitation hardening [20,21]. The TEM micrographs of Cu-Mg-Ce and Cu-Mg-Y alloys deformed at 800 °C and 0.01 s^{-1} are shown in Fig. 5(a) and Fig. 5(b), respectively. A lot of precipitations distributed in the matrix, which pinned in the subgrain boundaries and also in the dislocation. The selected area in Fig. 5(a) marked by the red circle is magnified, as shown in Fig. 5(c). It can be clearly seen that the secondary phase is pinning in the dislocation network and inhibits the movement of dislocations and grain boundaries. The emergence of substructures was impeded. Therefore, the occurrence of dynamic recrystallization was delayed and the flow stress increased. The diffraction pattern of the selected area of precipitations is shown in Fig. 5(d). According to the calculations, the secondary phase is CuP_2. In addition, Fig. 5(e) and (f) illustrate the TEM micrographs of Cu-Mg-Ce alloy deformed at 600 °C, 0.01 s^{-1} and 800 °C, 0.001 s^{-1}, respectively. In Fig. 5(e) exists a great amount of dislocations without precipitate compared with Fig. 5(b), which not only revels the condition of the precipitation occurs at 800 °C and 0.01 s^{-1}, but also corresponds to the flow stress curve in Fig. 2 that flow stress decreases with the increase of temperature [21,22]. Compared Fig. 5(f) with Fig. 5(c), the precipitates in Fig. 5(f) has a larger dimension in size. The reason is that lower strain rate provides sufficient time for the precipitates to grow up and form a coherent or semi-coherent relationship with the matrix. Therefore, the flow stress is reduced.

3.2. Critical strain

Dynamic recrystallization has a significant effect on decreasing the strain hardening. Therefore, it is important to determine the dynamic recrystallization onset of alloys under arbitrary deformation conditions. However, critical strain cannot be determined from the flow stress curves directly. For instance, only Cu-Mg alloy curve exhibits obvious dynamic recrystallization characteristics at 700 °C and 0.1 s^{-1} in Fig. 3(c). Poliak et al. [23–25] defined the strain hardening rate as $\theta = \partial\sigma/\partial\varepsilon$ by thermodynamics of irreversible processes and smoothed the flow stress curve with the ninth order polynomial regression. Poliak and Jonas proposed the following equation for easier distinguishing the critical strain in DRX:

$$\left(\frac{\partial\theta}{\partial\sigma}\right)_{\varepsilon} = \left(\frac{\partial \ln\theta}{\partial\varepsilon}\right)_{\varepsilon} \quad (1)$$

The -∂(lnθ)/∂ε-ε curve was presented in Fig. 6. The minimum value in the -∂(lnθ)/∂ε-ε curve with the null value of second derivative $\partial(\ln\theta)^2/\partial\varepsilon^2$ indicates the onset of DRX. According to the equation of Poliak and Jonas in Ref. [23]:

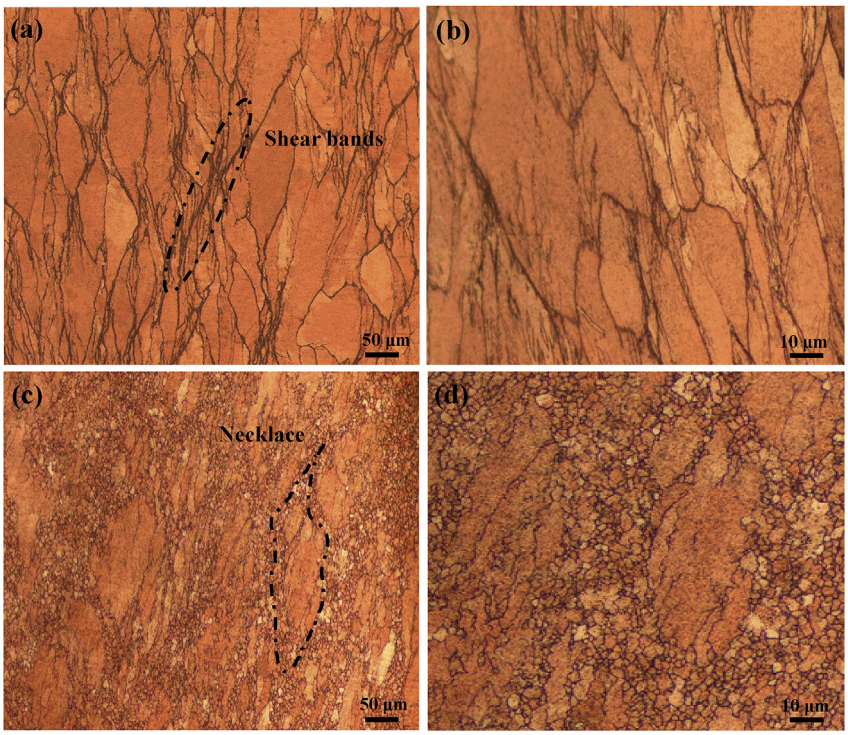

Fig. 4. Microstructure of Cu-Mg alloy deformed at 1 s^{-1} with the temperature of (a) 500 °C; (b) magnification of shear bans in (a); (c) 800 °C; (d) magnification of necklace in (c).

$$\frac{\partial}{\partial \varepsilon}\left(-\frac{\partial \ln \theta}{\partial \varepsilon}\right)=0 \tag{2}$$

The corresponding abscissa of the minimum point indicates the critical strain and also the DRX initiation. It can be seen that the Cu-Mg-Ce and Cu-Mg-Y alloys have a smaller critical strain value compared with the Cu-Mg alloy, which indicates that Ce and Y can delay the process of dynamic recrystallization for the Cu-Mg alloy. For instance, the critical strain value of Cu-Mg, Cu-Mg-Ce, and Cu-Mg-Y alloys deformed at 700 °C and 0.1 s^{-1} are 0.075, 0.1, and 0.14, respectively. Compared with Fig. 6(a), a higher critical strain value occurs at a lower temperature in Fig. 6(b) at 600 °C, which indicates that the higher temperature can accelerate the occurrence of dynamic recrystallization.

3.3. Microstructure evolution

The microstructure of Cu-Mg-Y alloy deformed at various temperatures and strain rate is shown in Fig. 7. As shown in Fig. 7(a), the grain elongation occurs parallel to the compressed direction deformed at 500 °C and 0.01 s^{-1}. Magnification of selected area in Fig. 7(a) is shown in Fig. 7(b), only shear bands tangled at grain boundaries. Due to the stored distortion energy at grain boundaries, the dynamic recrystallization grains preferentially nucleate at grain boundaries. Fig. 7(c) shows that the partial fine dynamic recrystallization grains appear at regions of localized shear bands at 600 °C and 0.01 s^{-1}. The magnification of the DRX grains is illustrated in Fig. 7(d). It is the typical characteristic of dynamic recrystallization [26].

At the deformation temperature of 700 °C and strain rate of 0.01 s^{-1}, the fine dynamic recrystallization grains are observed at original grain boundaries, as shown in Fig. 8 (a). The recrystallized grains are misaligned with the original grains, which makes the grain boundaries appear serrated during the process of grain boundary migration. Dynamic recrystallization grains engulf the surrounding grains and expand around them. The occurrence of necklace microstructure implies that strain-induced grain boundary migration is the dominant nucleation mechanism of dynamic recrystallization. It is well known that high temperature and low strain rate are beneficial for nucleation and growth of dynamic recrystallization grains [18,27]. Fig. 8(b) illustrates the microstructure of the Cu-Mg-Y alloy deformed at 800 °C and 0.01 s^{-1}. Numerous equiaxed grains are uniformly distributed in the grains and the original grains in the matrix have been completely replaced. At 800 °C and 0.01 s^{-1}, the work hardening and dynamic recrystallization are in equilibrium [28], and the flow stress reaches the steady state.

Fig. 8(c) shows the microstructure of the Cu-Mg-Y alloy deformed at 850 °C and 0.01 s^{-1}. A lot of mixed crystals with different crystal structure orientation can be seen. Since mixed crystal structure can lead to material fracture during hot deformation, it should be avoided. Fig. 8(d) shows the microstructure of the Cu-Mg-Y alloy deformed at 850 °C and 0.001 s^{-1}, where the grain coarsening occurs, which indicates that dynamic recrystallization fully completed at higher deformation temperature and lower strain rate. Similar microstructure evolution can be also observed in the Cu-Mg-Ce alloy, as illustrated in Figs. 9 and 10.

The microstructure evolution during hot deformation can be further discussed from the TEM microstructure. Fig. 11 shows TEM microstructure of the Cu-Mg-Y and Cu-Mg-Ce alloys deformed under various conditions. The Cu-Mg-Y alloy is shown in Fig. 11(a) and the Cu-Mg-Ce alloy in Fig. 11(b), all deformed at 500 °C and 0.01 s^{-1}, demonstrate that the dislocation density increases rapidly at low temperature deformation, and many dislocation cells exist inside the grains. Thus, the increased dislocation density and dislocation tangles cause work hardening. Finally, the work hardening leads to increased flow stress.

Due to the temperature increase, dynamic recrystallization controls the process of hot deformation. Many subgrains appear in

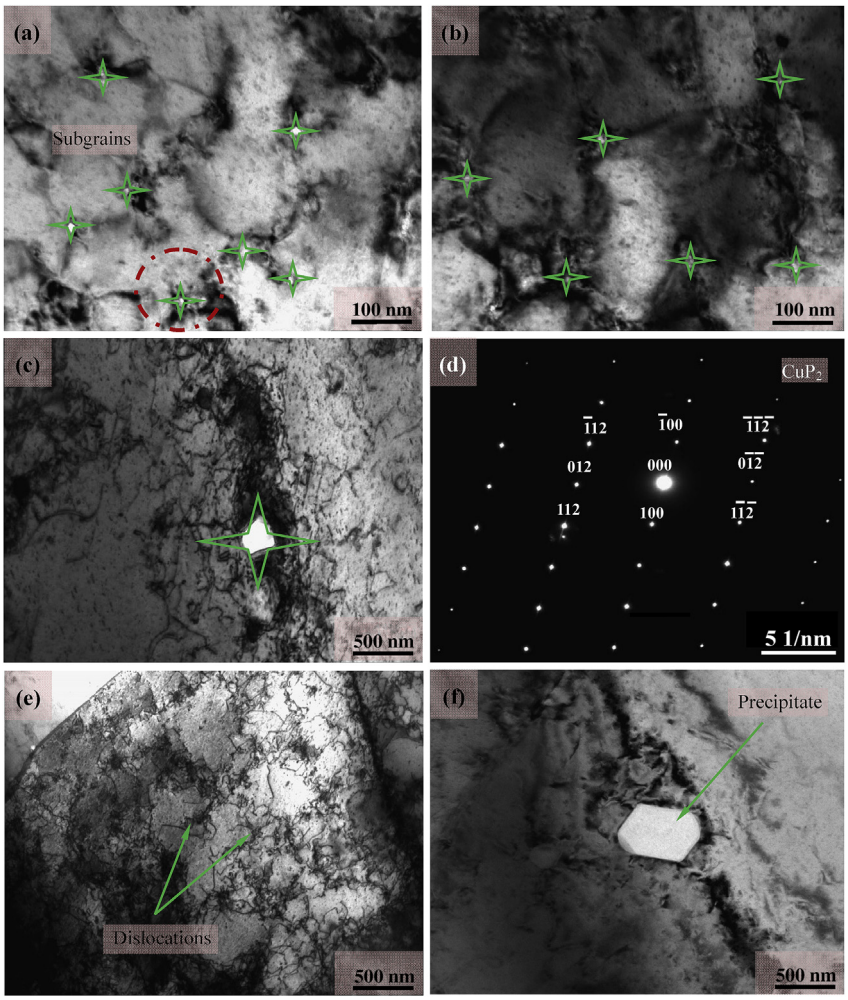

Fig. 5. TEM micrographs of (a) Cu-Mg-Ce alloy; (b) Cu-Mg-Y alloy deformed at 800 °C and 0.01 s^{-1}; (c) magnification of red circled area in (a); (d) SAED pattern of secondary phase in (c); Cu-Mg-Ce alloy deformed at (e) 600 °C and 0.01 s^{-1}; (f) 800 °C and 0.001 s^{-1}. (For interpretation of the references to colour in this figure legend, the reader is referred to the Web version of this article.).

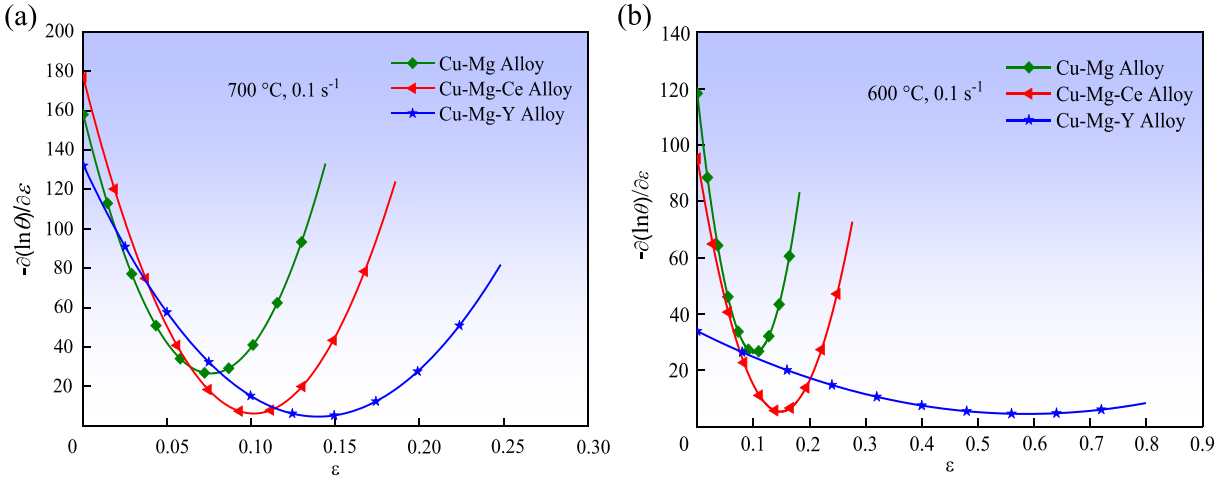

Fig. 6. Strain hardening rate $-\partial(\ln\theta)/\partial\varepsilon$-$\varepsilon$ curve of Cu-Mg, Cu-Mg-Ce and Cu-Mg-Y alloys deformed at (a) 700 °C, 0.1 s^{-1}; (b) 600 °C, 0.1 s^{-1}.

the matrix of the Cu-Mg-Y and Cu-Mg-Ce alloys deformed at 800 °C and 0.01 s^{-1} as shown in Fig. 11(c) and (d), respectively. The high-density dislocation area produced in the process of work hardening reduced the dislocation density by multilateralization and caused the elimination of opposite sign dislocations, and then formed subgrains and regular subgrain boundaries, thus effectively

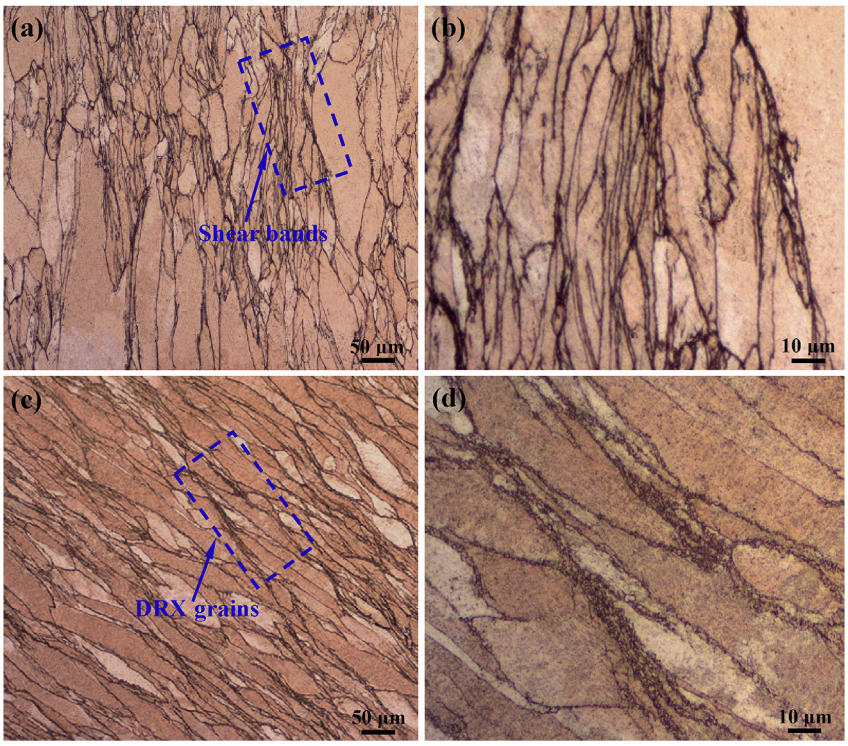

Fig. 7. Microstructure of Cu-Mg-Y alloy at different deformation conditions (a) 500 °C, 0.01 s^{-1}; (b) magnification of shear bans in (a); (c) 600 °C, 0.01 s^{-1}; (d) magnification of DRX grains in (c).

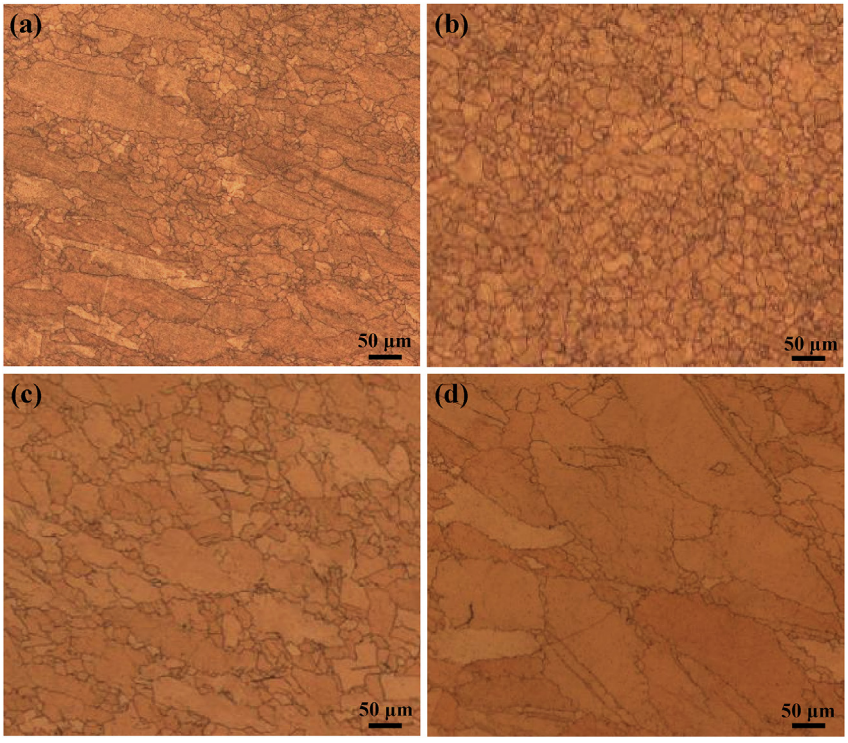

Fig. 8. Microstructure of Cu-Mg-Y alloy at different deformation conditions (a) 700 °C, 0.01 s^{-1}; (b) 800 °C, 0.01 s^{-1}; (c) 850 °C, 0.01 s^{-1}; (d) 850 °C, 0.001 s^{-1}.

eliminating work hardening. The TEM microstructure of the Cu-Mg-Y and Cu-Mg-Ce alloys deformed at 850 °C with the 0.001 s^{-1} strain rate is shown in Fig. 11(e) and (f). It indicated that the alloy is entirely composed of the high angle grain boundaries. Thus, the dynamic recrystallization is completed at this condition. This phenomenon proves that high temperature and low strain rate are more conducive to dynamic recrystallization.

As mentioned above, precipitates increased the flow stress and

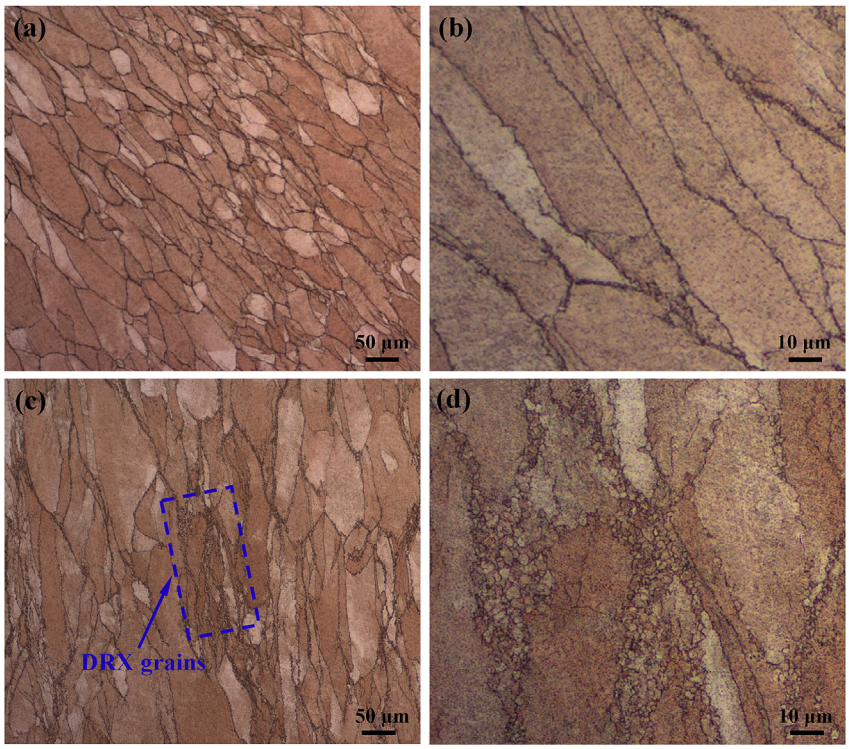

Fig. 9. Microstructure of Cu-Mg-Ce alloy at different deformation conditions (a) 500 °C, 0.01 s^{-1}; (b) magnification of shear bands in (a); (c) 600 °C, 0.01 s^{-1}; (d) magnification of DRX grains in (c).

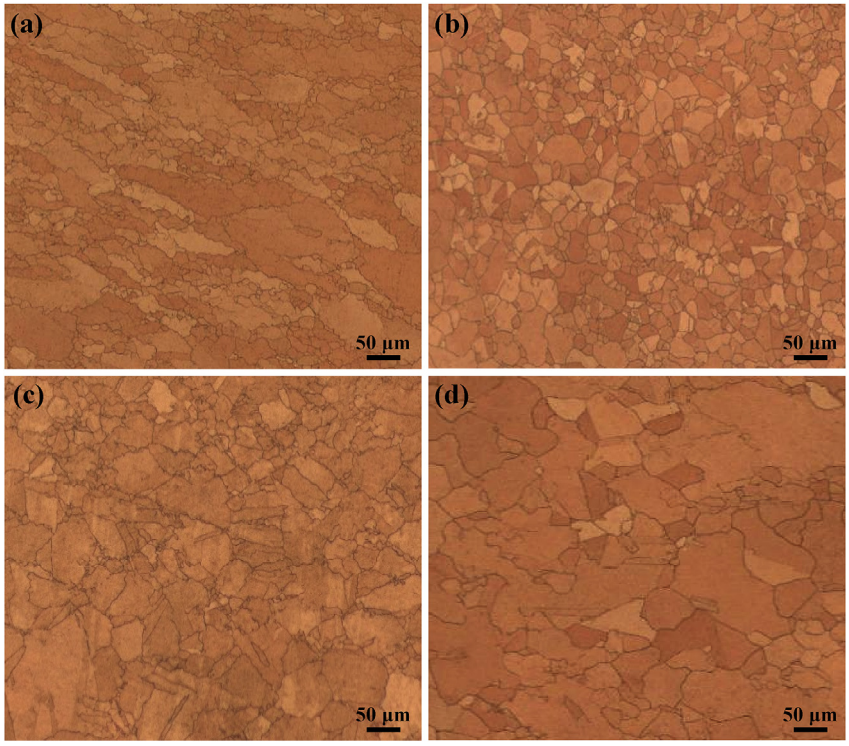

Fig. 10. Microstructure of Cu-Mg-Ce alloy at different deformation conditions (a) 700 °C, 0.01 s^{-1}; (b) 800 °C, 0.01 s^{-1}; (c) 850 °C, 0.01 s^{-1}; (d) 850 °C, 0.001 s^{-1}.

delayed the dynamic recrystallization process. Fig. 12 illustrates the TEM microstructure of the Cu-Mg alloy at 800 °C and 0.01 s^{-1}. Only high angle grains appear in the matrix and dynamic recrystallization is completed. However, when Fig. 12 is compared with Fig. 11(c) and (d), it is obvious that no subgrains are present in Fig. 12. This indicated that Ce and Y delay the DRX process and

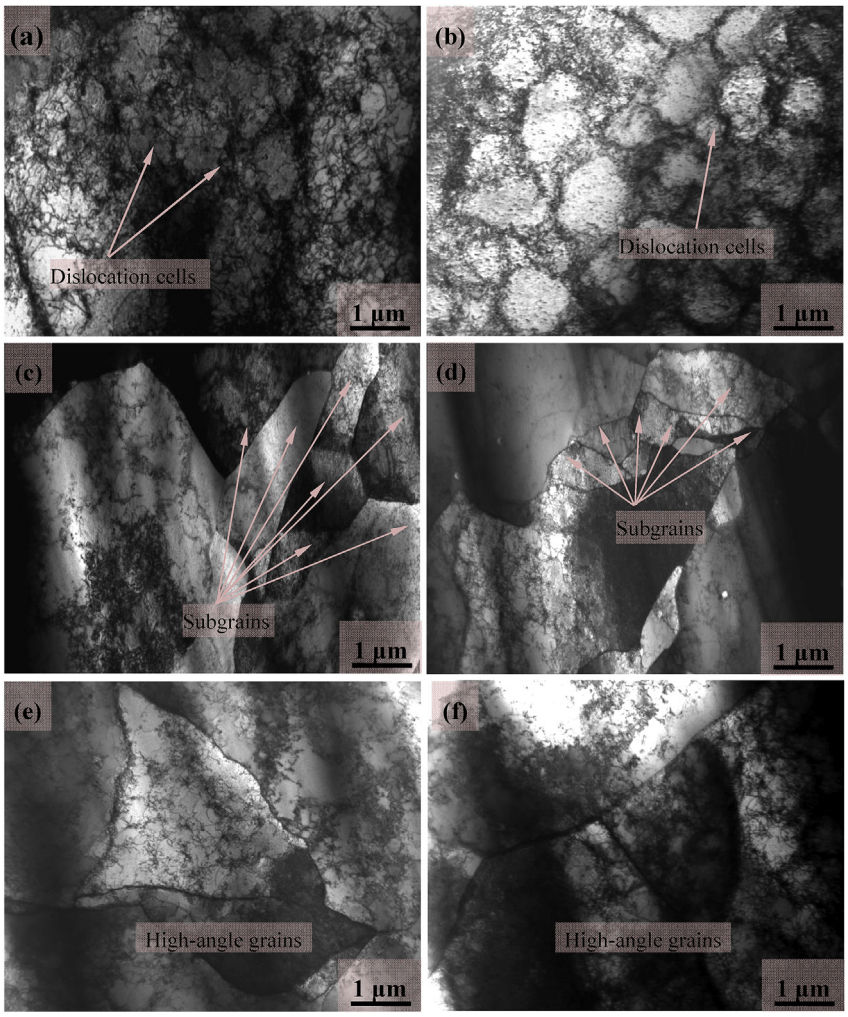

Fig. 11. TEM microstructure of samples deformed at: (a) Cu-Mg-Y, 500 °C, 0.01 s^{-1}; (b) Cu-Mg-Ce, 500 °C, 0.01 s^{-1}; (c) Cu-Mg-Y, 800 °C, 0.01 s^{-1}; (d) Cu-Mg-Ce, 800 °C, 0.01 s^{-1}; (e) Cu-Mg-Y, 850 °C, 0.001 s^{-1}; (f) Cu-Mg-Ce, 850 °C, 0.001 s^{-1}.

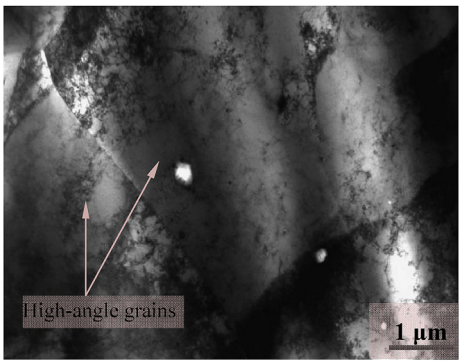

Fig. 12. TEM microstructure of Cu-Mg alloy deformed at 800 °C and 0.01 s^{-1}.

increase the recrystallization temperature.

4. Discussion

4.1. Refining effect of Ce and Y addition on Cu-Mg alloy

Fig. 13 illustrates the microstructure of Cu-Mg, Cu-Mg-Ce, and Cu-Mg-Y alloys after solution treatment at 900 °C for 2 h. It is seen from Fig. 13(a) that there are mainly coarse grains in the matrix of the Cu-Mg alloy. The microstructure of Cu-Mg-Ce and Cu-Mg-Y alloys is shown in Fig. 13(b) and (c). Compared with Fig. 11(a), the grains of Cu-Mg-Ce and Cu-Mg-Y alloys are obviously refined. In addition, the grain boundary area is increased and a large number of equiaxed annealing twins can be seen in Fig. 13(b) and (c), which inhibit dislocation movement [29]. Finally, flow stress for Cu-Mg-Ce and Cu-Mg-Y alloys increase.

4.2. Secondary phase resulting from Ce and Y addition

It has been proven that the addition of rare earth elements promotes secondary phase precipitation [30]. Different types of secondary phases have been found in previous research. Cheng et al. [31] found Cr-rich precipitates in the Cu-Cr-Zr-Mg alloy aged at 400 °C. Chaim et al. [32] researched the Cu-Mg alloys and proved that Cu_2Mg precipitates were formed during aging above 450 °C. Maki et al. [33] found the existence of Cu_2Mg precipitates in the Cu-6Mg alloy aged at 400 °C. In this experiment, after hot deformation at 850 °C and 0.001 s^{-1}, a large number of fine secondary phases were dispersed within the grains of Cu-Mg-Y and Cu-Mg-Ce alloys, as shown in Fig. 14(a) and Fig. 14(b), respectively. The selected area diffraction patterns are shown in Fig. 14(c) for the Cu-Mg-Y alloy and Fig. 14(d) for the Cu-Mg-Ce alloy. The secondary phases are

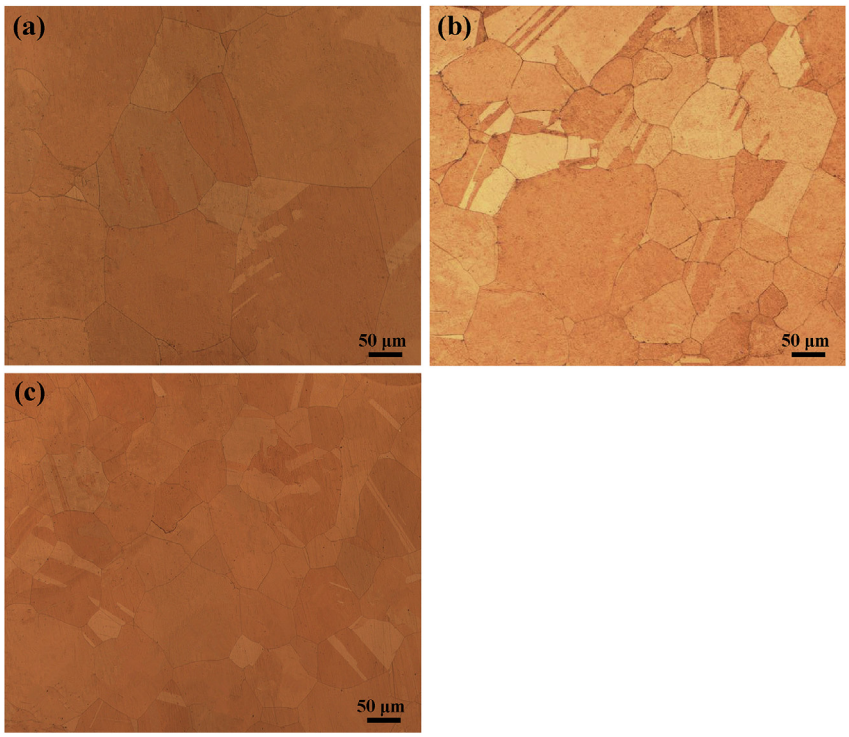

Fig. 13. Microstructure of (a) Cu-Mg; (b) Cu-Mg-Ce; (c) Cu-Mg-Y alloys after solution treatment at 900 °C for 2 h.

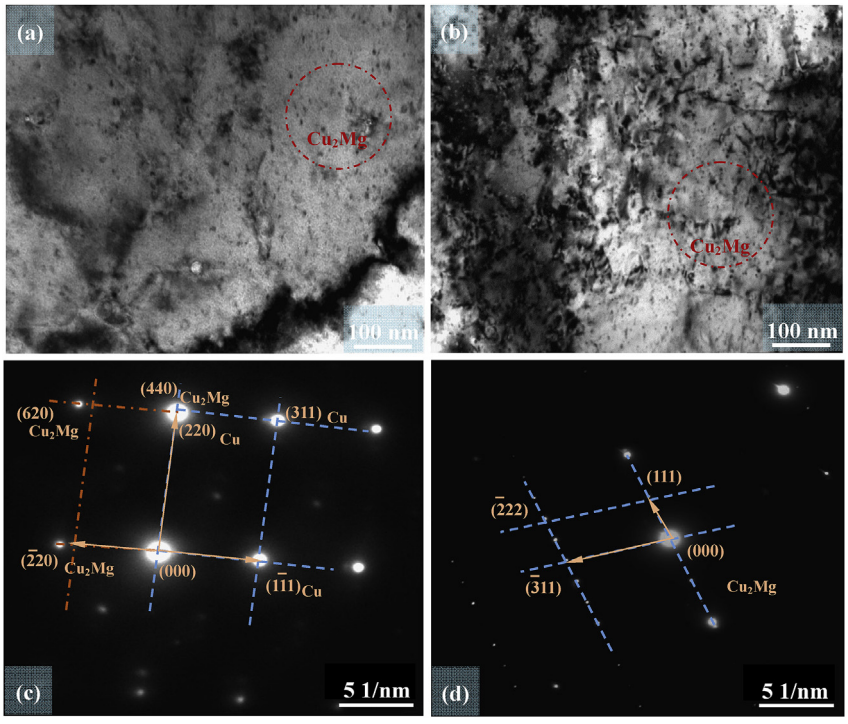

Fig. 14. TEM micrographs of secondary phases from samples deformed at 850 °C and 0.001 s^{-1} in: (a) Cu-Mg-Y alloy, (b) Cu-Mg-Ce alloy; (c) SAED pattern of secondary phases in (a); (d) SAED pattern of secondary phases in (b).

determined to be Cu_2Mg.

Furthermore, a new phase was observed in the Cu-Mg-Y alloy deformed at 800 °C and 0.01 s^{-1}, which is shown in Fig. 15(a). Based on the selected area diffraction patterns, it is determined to be face centered cubic (fcc) YP. Corresponding diffraction pattern analysis is shown in Fig. 15(b).

4.3. Twinning mechanism

Homogenization annealing and thermal deformation were

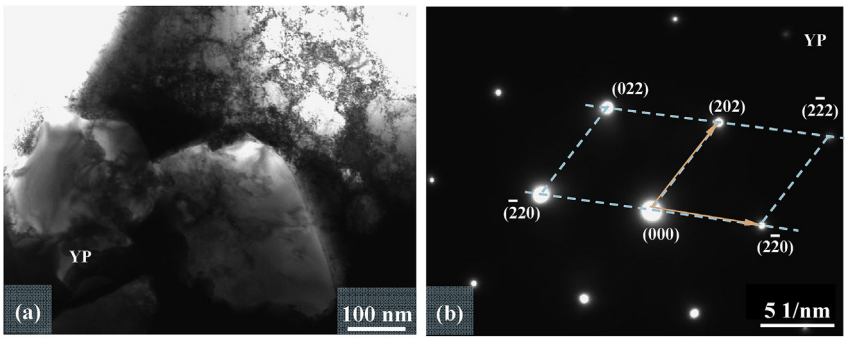

Fig. 15. TEM microstructure of Cu-Mg-Y alloy deformed at 800 °C and 0.01 s^{-1}; (b) SAED pattern of secondary phase.

carried out in this experiment. As shown in Fig. 2, no twins can be found in the as-cast structure of the three alloys. However, annealing twins appear in the annealed structure. The annealing twins are formed in the process of grain growth. When the grains migrate through grain boundaries and grow, the stacking sequence of atomic layers at the grain boundary angle accidentally staggers, resulting in a coherent twin interface. While the continuous migration and growth of the twin interface at large angle grain boundary, the atoms stagger again at the original interface and return to the normal stacking sequence, and then a second coherent twin interface will be formed, finally formed an annealed twin band. In addition, another kind of twins appeared after thermal deformation showed in Fig. 16. When dislocation slip is blocked during thermal deformation, twins will germinate in the stress concentration region and control the slippage in crystals. Twins change the crystal orientation and then promote the dislocation slippage in the crystal. Twins will reduce the mean free path of dislocation and play a role of hardening.

It has been mentioned that rare earth elements have a pinning effect on dislocation, and dislocation slip is more difficult. Therefore, the alloy incorporating dilute elements will slip in a twinning way. The twins with addition of rare earth elements are obviously more than without. According to Eq. (3):

$$d = \frac{Gb_1b_2}{2\pi r} \tag{3}$$

Here d is width of extended dislocation, b_1, b_2 are two Bernstein vectors of Shockley dislocation, r is the stacking fault energy. Increasing the number of twins means increasing the width between extended dislocations. As a result, the stacking fault energy decreases. The increasing of the width of extended dislocations widths is more unfavorable for dislocation climb or cross slip. Therefore, the number of twins increase further.

A large number of twins appear in the Cu-Mg-Y alloy deformed at 800 °C and 0.01 s^{-1}. Due to the large number of twin boundaries, the movement of dislocations and subgrains is hindered, which increases flow stress and delays the dynamic recrystallization process [34]. Many dislocations can be seen in the structure of twins. Fig. 16(a) and (b) are slightly different in the two structures of twins. The dislocations seen in Fig. 16(a) are mainly on slip planes

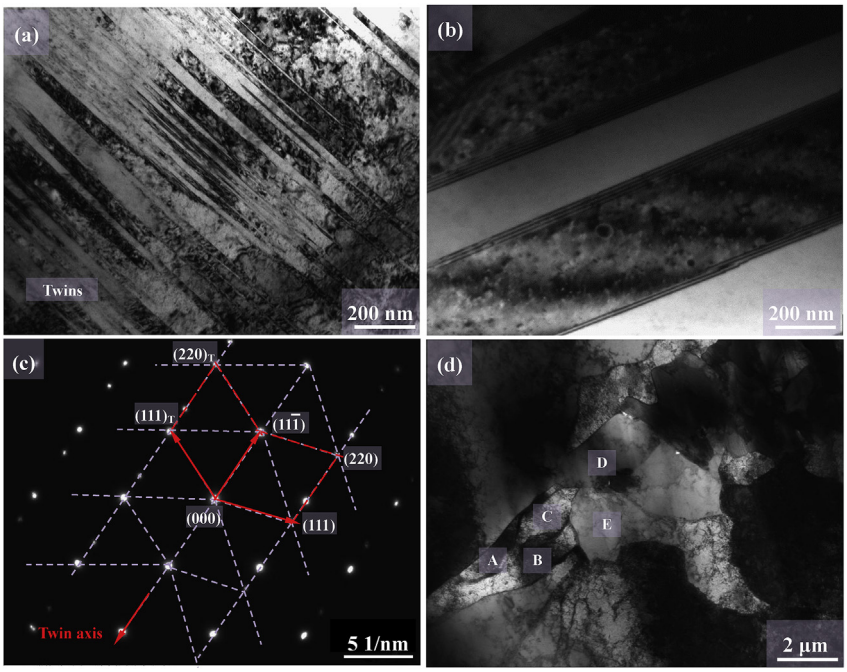

Fig. 16. TEM micrographs of 800 °C deformed Cu-Mg-Y alloy at 0.01 s^{-1} strain rate (a), (b); 0.001 s^{-1} strain rate (d); (c) SAED pattern of (a).

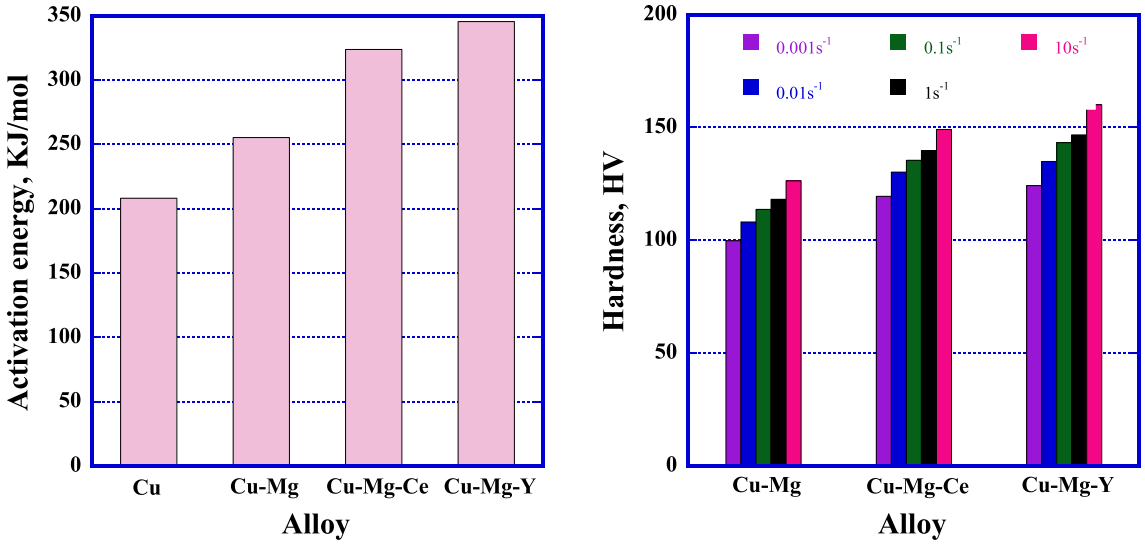

Fig. 17. (a) Activation energy of different alloys; (b) hardness of Cu-Mg, Cu-Mg-Ce, and Cu-Mg-Y alloys at 700 °C.

and contain sharp twin boundaries, and some dislocations are entangled at the boundary of the twinning zone. As for Fig. 16(b), the dislocations appear as parallel shade regions due to the difference in orientation of different grains. Myshlyaev et al. [35] have obtained similar conclusions. The crystal structure of the twins for Cu-Mg-Y is shown in Fig. 16(c). It is worth mentioning that many fine grains are caused by twins intersecting around subgrains in the Cu-Mg-Y matrix deformed at 800 °C and 0.001 s^{-1} strain rate, are marked A, B, C, D, and E in Fig. 16(d). The increased number of twins implies more twin boundaries, which enhance grain refinement [36,37].

Grain refinement and secondary phase pinning effects greatly improve the flow stress. The precipitation of the secondary phase reduces the effective deformation stress [18] and leads to an increase in alloy activation energy, delaying the dynamic recrystallization process and increasing the high temperature stability of the alloy [38]. The effects of Ce and Y addition on activation energy can be influenced by constitutive characteristics. Sellars and Mctegart [39] established the hyperbolic-sine Arrhenius equation:

$$\dot{\varepsilon} = A\left[\sinh(\alpha\sigma)^n \exp\left(-\frac{Q}{RT}\right)\right] \quad (4)$$

Here A, α are the material's constants, R is the universal gas constant, Q is the activation energy, σ is the peak flow stress, T is the temperature, and $\dot{\varepsilon}$ is the strain rate.

Fig. 17(a) describes the activation energy of Cu-Mg, Cu-Mg-Ce, and Cu-Mg-Y alloys using data taken from Ref. [19]. The activation energy of the Cu-Mg-Ce and Cu-Mg-Y alloys was increased by 27% and 35%, respectively. Meanwhile, compared with pure copper, the activation energy of the Cu-Mg, Cu-Mg-Ce, and Cu-Mg-Y alloys is much higher. In other words, the high activation energy indicates that more deformation energy is needed for dynamic recrystallization. In addition, the dynamic recrystallization deformation temperature is increased, which indicates the Ce or Y copper alloys have better high-temperature stability. Fig. 17(b) illustrates that the Cu-Mg-Ce and Cu-Mg-Y alloys have higher hardness than the Cu-Mg alloy after deformation at 700 °C with various strain rates. This indicates that the addition of Y and Ce greatly strengthens the Cu-Mg alloy. Furthermore, Y addition promotes the formation of twins and makes the microstructure more uniform in the hot deformation process. Cu-Mg-Y alloy has higher hardness and thermal deformation activation energy compared with the Cu-Mg and Cu-Mg-Ce alloys, which indicates that the Cu-Mg-Y alloy has better stability at high temperature.

In addition, Y promotes the formation of twins and makes the microstructure more uniform in the hot deformation process. The Cu-Mg-Y alloy has higher hardness and thermal deformation activation energy compared with the Cu-Mg and Cu-Mg-Ce alloys, which indicates that the Cu-Mg-Y alloy has better hot processing performance.

5. Conclusions

Hot deformation behavior of the three alloys (Cu-Mg, Cu-Mg-Ce, and Cu-Mg-Y) were investigated at deformation temperature ranging from 500 °C to 850 °C and strain rate ranging from 0.001 s^{-1} to 10 s^{-1}. The effects of Ce and Y addition on Cu-Mg alloy were discussed. The main conclusions are as follows:

(1) Flow stress increases with strain rate and decreases with deformation temperature, and dynamic recrystallization dominates the hot deformation process at high temperature.
(2) Addition of Ce and Y caused Cu-Mg alloy grain refinement, which improved the flow stress and hardness of the Cu-Mg alloy. At the same time, Ce and Y enhance the activation energy of Cu-Mg alloy by 27% and 35%, respectively. Furthermore, addition of Ce and Y increases the critical strain and delays the occurrence of dynamic recrystallization.
(3) The precipitation of the CuP_2 and Cu_2Mg secondary phases enhanced the strength and hardness of Cu-Mg-Ce and Cu-Mg-Y by pinning dislocations and subgrains. New precipitate YP was obtained by the addition of Y to the Cu-Mg-Y alloy.
(4) Twinning occurs and causes refinement of the alloys with Y added. Dispersion strengthening and fine-grain strengthening become the main strengthening mechanisms during deformation of alloys with added Ce or Y. The temperature of recrystallization increases with the occurrence of dynamic recrystallization, which improves the high temperature stability of the material.

Acknowledgements

This work was supported by the Henan University Scientific and Technological Innovation Talent Support Program (18HASTIT024), China, the National Natural Science Foundation of China (U1704143), China, the Open Cooperation Project of Science and Technology of the Hennan Province (172106000058 and 182106000018), China, and by the National Science Foundation (IRES 1358088), USA.

References

[1] G. Yang, L. Zhou, Y. Yuan, L. Qian, Microstructure, mechanical properties and electrical conductivity of Cu-0.3Mg-0.05Ce alloy processed by equal channel angular pressing and subsequent annealing, J. Alloys Compd. 640 (2015) 347–354.
[2] C.D. Xia, Y.L. Jia, W. Zhang, K. Zhang, Q.Y. Dong, G.Y. Xu, M.P. Wang, Study of deformation and aging behaviors of a hot rolled-quenched Cu-Cr-Zr-Mg-Si alloy during thermomechanical treatments, Mater. Des. 39 (2012) 404–409.
[3] I.S. Batra, G.K. Dey, U.D. Kulkarni, S. Banerjee, Precipitation in a Cu-Cr-Zr alloy, Mater. Sci. Eng. A 356 (2003) 32–36.
[4] A. Chbihi, X. Sauvage, D. Blavette, Atomic scale investigation of Cr precipitation in copper, Acta Mater. 60 (2012) 4575–4585.
[5] S. Spigarelli, M. EI Mehtedi, M. Cabibbo, F. Gabrielli, D.C. ccarelli, High temperature processing of brass: constitutive analysis of hot working of Cu-Zn alloys, Mater. Sci. Eng. A 615 (2014) 331–339.
[6] S. Spigarelli, M. EI Mehtedi, A New constitutive model for the plastic flow of metals at elevated temperatures, J. Mater. Eng. Perform. 23 (2014) 658–665.
[7] S. Spigarelli, M. EI Mehtedi, P. Ricci, C. Mapelli, Constitutive equations for prediction of the flow behaviour of duplex stainless steels, Mater. Sci. Eng. A 527 (2010) 4218–4228.
[8] L.Y. Jiang, W.J. Huang, D.F. Zhang, F. Guo, H.S. Xue, J.Y. Xu, F.S. Pan, Effect of Sn on the microstructure evolution of AZ80 magnesium alloy during hot compression, J. Alloys Compd. 727 (2017) 205–214.
[9] Q.Y. Dong, L.N. Shen, F. Cao, Y.L. Jia, K.J. Liao, M.P. Wang, Effect of thermo-mechanical processing on the microstructure and properties of a Cu-Fe-P Alloy, Mater. Eng. Perform. 24 (2015) 1531–1539.
[10] D. Janovszky, K. Tomolya, M. Sveda, A. Sycheva, G. Kaptay, Effect of Y and Ni addition on liquid immiscibility in Cu-Zr-Ag ternary alloys, J. Alloys Compd. 615 (2014) S616–S620.
[11] N. Stanford, D. Atwell, A. Beer, C. Davies, M.R. Bamett, Effect of microalloying with rare-earth elements on the texture of extruded magnesium-based alloys, Scr. Mater. 59 (2008) 772–775.
[12] N. Stanford, Micro-alloying Mg with Y, Ce, Gd and La for texture modification-A comparative study, Mater. Sci. Eng. A 527 (2010) 2669–2677.
[13] H.H. Li, S.H. Zhang, Y. Chen, M. Cheng, H.W. Song, Effects of small amount addition of rare earth Ce on microstructure and properties of cast pure copper, J. Mater. Eng. Perform. 24 (2015) 2857–2865.
[14] Y. Zhang, Z. Chai, A.A. Volinsky, B.H. Tian, H.L. Sun, P. Liu, Processing maps for the Cu-Cr-Zr-Y alloy hot deformation behavior, Mater. Sci. Eng. A 662 (2016) 320–329.
[15] J. Chen, Y. Zhang, J.P. He, K.F. Yao, B.C. Wei, G.L. Chen, Metallographic analysis of Cu-Zr-Al bulk amorphous alloys with yttrium addition, Scr. Mater. 54 (2006) 1351–1355.
[16] H. Mirzadeh, M.H. Parsa, Hot deformation and dynamic recrystallization of NiTi intermetallic compound, J. Alloys Compd. 614 (2014) 56–59.
[17] A. Rohatgi, K.S. Vecchio, G.T. Gray, The influence of stacking fault energy on the mechanical behavior of Cu and Cu-Al alloys: deformation twinning, work hardening, and dynamic recovery, Metall. Mater. Trans. A 32 (2001) 135–145.
[18] L. Qian, L. Zhou, A.Y. Zhu, W.T. Qiu, S.Q. Liang, The transformation behavior of Cu-8.0Ni-1.8Si-0.6Sn-0.15Mg alloy during isothermal heat treatment, Mater. Char. 62 (2011) 904–911.
[19] B.J. Wang, Y. Zhang, B.H. Tian, J.C. An, A.A. Volinsky, H.L. Sun, Y. Liu, K.X. Song, Effects of Ce addition on the Cu-Mg-Fe alloy hot deformation behavior, Vacuum 155 (2018) 594–603.
[20] G.L. Ji, Q. Li, L. Li, A physical-based constitutive relation to predict flow stress for Cu-0.4Mg alloy during hot working, Mater. Sci. Eng. A 615 (2014) 247–254.
[21] A.K. Shukla, S.V.S.N. Murty, S.C. Sharma, K. Mondal, Constitutive modeling of hot deformation behavior of vacuum hot pressed Cu-8Cr-4Nb alloy, Mater. Des. 75 (2015) 57–64.
[22] D.J. Li, Y.R. Feng, S.Y. Song, Q. Liu, Q. Bai, F.Z. Ren, F.S. Shangguan, Influences of silicon on the work hardening behavior and hot deformation behavior of Fe-25 wt%Mn-(Si, Al) TWIP steel, J. Alloys Compd. 618 (2015) 768–775.
[23] E.I. Poliak, J.J. Jonas, A one-parameter approach to determining the critical conditions for the initiation of dynamic recrystallization, Acta Mater. 44 (1996) 127–136.
[24] J.J. Jonas, E.I. Poliak, The critical strain for dynamic recrystallization in rolling mills[J], Mater. Sci. Forum 426 (2003) 57–66.
[25] E.I. Poliak, J.J. Jonas, Critical strain for dynamic recrystallization in variable strain rate hot deformation, ISIJ Int. 43 (2003) 692–700.
[26] L. Zhang, Z. Li, Q. Lei, W.T. Qiu, H.T. Luo, Hot deformation behavior of Cu-8.0Ni-1.8Si-0.15Mg alloy, Mater. Sci. Eng. A 528 (2011) 1641–1647.
[27] Q. Lei, Z. Li, M.P. Wang, L. Zhang, S. Gong, Z. Xiao, Z.Y. Pan, Phase transformations behavior in a Cu-8.0Ni-1.8Si alloy, J. Alloys Compd. 509 (2011) 3617–3622.
[28] Y.T. Wu, Y.C. Liu, C. Li, X.C. Xia, Y. Huang, H.J. Li, Deformation behavior and processing maps of Ni_3Al-based superalloy during isothermal hot compression, J. Alloys Compd. 712 (2017) 687–695.
[29] A.P. Zhilyaev, I. Shakhova, A. Morozova, A. Belyakov, R. Kaibyshev, Grain refinement kinetics and strengthening mechanisms in Cu-0.3Cr-0.5Zr alloy subjected to intense plastic deformation, Mater. Sci. Eng. A 654 (2016) 131–142.
[30] N. Liu, L. Zhou, G.Y. Xu, Z. Feng, S.Q. Liang, Hot deformation behavior and cold workability of Cu-12Mn-13Zn-1Sn-1Al-0.1Si-0.1Ce alloy with white chromaticity, Mater. Sci. Eng. A 553 (2012) 67–73.
[31] J.Y. Cheng, B. Shen, F.X. Yu, Precipitation in a Cu-Cr-Zr-Mg alloy during aging, Mater. Char. 81 (2013) 68–75.
[32] R. Chaim, J. Pelleg, M. Talianker, TEM observation of a Cu-Mg age-hardenable alloy, J. Mater. Sci. 22 (1987) 1609–1612.
[33] K. Maki, Y. Ito, H. Matsunaga, H. Mori, Solid-solution copper alloys with high strength and high electrical conductivity, Scr. Mater. 68 (2013) 777–780.
[34] R. Mishnev, I. Shakhova, A. Belyakov, R. Kaibyshev, Deformation microstructures, strengthening mechanisms, and electrical conductivity in a Cu-Cr-Zr alloy, Mater. Sci. Eng. A 629 (2015) 29–40.
[35] M.M. Myshlyaev, H.J. Mcqueen, A. Mwembela, E. Konopleva, Twinning, dynamic recovery and recrystallization in hot worked Mg-Al-Zn alloy, Mater. Sci. Eng. A 337 (2002) 121–133.
[36] Y. Chino, K. Kimura, M. Mabuchi, Twinning behavior and deformation mechanisms of extruded AZ31 Mg alloy, Mater. Sci. Eng. A 486 (2008) 481–488.
[37] P.A. Juan, C. Pradalier, S. Berbenni, R.J. McCabe, C.N. Tomé, L. Capolungo, A statistical analysis of the influence of microstructure and twin-twin junctions on twin nucleation and twin growth in Zr, Acta Mater. 95 (2015) 399–410.
[38] D.P. Lu, J. Wang, W.J. Zeng, Y. Liu, L. Lu, B.D. Sun, Study on high-strength and high-conductivity Cu-Fe-P alloys, Mater. Sci. Eng. A 421 (2006) 254–259.
[39] C.M. Sellars, W.J. Mctegart, On the mechanism of hot deformation, Acta Metall. 14 (1966) 1136–1138.